Journal of Applied Polymer Science

Superporous Collagen-Sericin Scaffolds

Adriana Lungu,[1] Madalina G. Albu,[2] Izabela Cristina Stancu,[1] Nicoleta M. Florea,[1] Eugeniu Vasile,[1] Horia Iovu[1]

[1]Advanced Polymer Materials Group, Department of Bioresources and Polymer Science, University Politehnica of Bucharest, Bucharest, Romania

[2]Collagen Department, INCDTP-Division Leather and Footwear Research Institute, Bucharest, Romania

Correspondence to: H. Iovu (E-mail: iovu@tsocm.pub.ro)

ABSTRACT: Superporous materials based on two proteins, collagen and sericin were synthesized by freeze-drying considering various ratios between the two proteins. To evaluate the influence of sericin content on the structure/properties relationship, the obtained scaffolds were further characterized using spectroscopic analysis, thermal, and mechanical techniques. Scanning electron microscopy was used to investigate the morphological structure of the scaffolds and the swelling properties as well as the stability of the scaffolds were also assessed. © 2012 Wiley Periodicals, Inc. J. Appl. Polym. Sci. 000: 000–000, 2012

KEYWORDS: porous materials; proteins; structure-property relations

Received 5 September 2011; accepted 20 April 2012; published online
DOI: 10.1002/app.37934

INTRODUCTION

The promising next generation of biocompatible scaffolds that mimic extracellular matrix has attracted much attention over the last decades. Natural polymers are generally considered biocompatible for tissue engineering applications. The protein-based polymers have the advantage of mimicking many characteristics of extracellular matrix which allows for different cell types to develop and proliferate. The protein polymer structure is consisting of 20 distinct amino acids linked by amide (or peptide) bonds. The differences between characteristics of protein are given by side chains and their distribution along protein backbone.[1,2]

Collagen is one of the most widely used biomaterials due to its excellent biocompatibility and biodegradability properties, well established structure and biological characteristics. Type I collagen consists of three α-helix polypeptide chains of $((Gly)\text{-}X\text{-}Y)_n$ amino acids, where Gly is glycine, X is proline, and Y is hydroxyproline, arranged in characteristic sequences to form a unique conformational structure of triple helix.[3] Hydroxyproline is characteristic only for collagen and it confers stability, especially through intermolecular hydrogen bonds.

Extracted as aqueous solution or gel, type I collagen can be processed in different forms such as: medical devices, artificial implants, or support for drug release and scaffolds for tissue regeneration that have an important role in medicine today.[4–8]

Sericin is an adhesive silk protein synthesized by silkworm and acts as a glue to envelop the fibroin fibers in the formation of a cocoon. Silk sericin (SS) is a highly hydrophilic macromolecular protein being composed of 18 amino acids, among which the polar amino acids with hydroxyl and amino groups such as serine, lysine, and aspartic acid account for 72%. The secondary structure of SS is various due to the obtaining conditions, being mainly an amorphous random coil (easily water soluble) and to a less extent a β sheet organized structure (more difficult to dissolve in water).[9–11] Aramwit et al.[12] previously reported that SS is nontoxic to fibroblast cells and enhances wound healing by promoting collagen production in wounds.[13] Earlier reports claimed that SS could be a source of immunogenic reactions; however, few studies have investigated the use of SS in the tissue engineering field. SS has been identified as the cause of the inflammatory response to undegummed silkworm silk, but is strongly influenced by the physical association with fibroin-silk and a significant activation of macrophages occurs.[14,15] SS itself generates very low immune responses and nowadays is commonly used as a value added product.[16]

The reactive functional groups (hydroxyl, carboxyl, and amino) of SS offer the possibility to react with other polymers (both natural and synthetic). In the last decade, many researchers have focused on development of novel materials using SS and natural (chitosan, keratin, cellulose) or synthetic (polyethyleneglycol, polyvinylalcohol) polymers into applicable forms for

various applications.[17–22] Recent studies have found that SS has excellent features such as antioxidative, antibacterial, UV resistant, moisture-absorbing and -desorbing properties, enzymes or drugs immobilization.[23–27] SS films support also the attachment and growth of L929 murine fibroblasts and cultured human skin fibroblasts.[28,29] SS forms fragile materials that are not suitable for use in medical applications, but Mandal et al.[30] demonstrated that after blending with gelatin, it can form a scaffold and be a good candidate for tissue engineering applications.

Hence, SS could be a promising natural resource for developing novel protein-based biomaterials with various cosmetic, medical, and pharmaceutical applications. Moreover, due to its proteic nature SS is also susceptible to the action of proteolytic enzymes present in the human body.[11] Very recently, Keskin and coworkers[31] reported the synthesis of sericin/collagen membranes and suggest their use as wound dressing material if sericin ratio is less than or equal to the collagen component.

The main objective of this study was to synthesize and characterize novel three-dimensional (3D) scaffolds consisting in two protein-based polymers: collagen and sericin. The scaffolds with different sericin amounts were prepared by crosslinking with glutaraldehyde (GA) followed by freeze-drying. The resulting scaffolds were characterized by attenuated total reflection Fourier transform infrared (ATR-FTIR). To further investigate the effect of SS on the thermal behavior of the scaffolds thermogravimetric analysis (TGA)/derivative thermogravimetry (DTG) and differential scanning calorimetry (DSC) were performed. Scanning electron microscopy (SEM), swelling ratio (SR), and collagenase degradation were further used to analyze the structure/properties relationship. To the best of our knowledge, there are no reports on the influence of collagen: sericin ratio on the thermal properties, morphology, swelling degree, and *in vitro* degradation of the two proteins-based scaffolds. The obtained superporous materials could be used as scaffolds for different cell types or drug delivery systems depending on the ratio between collagen and sericin.

EXPERIMENTAL

Materials

Type I fibrillar collagen was extracted from calf hide by acid and alkaline treatments as previously described.[5] Collagen (Coll) gel with a concentration of 1.54% (w/w) was further prepared. Sericin silkworm (SS) was purchased from Sigma-Aldrich (Japan). Bicinchoninic acid (BCA) kit for protein determination was purchased from Sigma Aldrich; the kit contained reagent A: BCA solution and reagent B: 4% (w/v) $CuSO_4 \times 5\ H_2O$ solution. Bovine serum albumin (BSA) (concentration 1 mg/ml in 0.15 M NaCl) was provided as control sample in the BCA Protein Assay kit. Collagenase of *Clostridium histolyticum* was received from Sigma-Aldrich and GA from Merck (Germany). Sodium hydroxide and phosphate buffer solution (PBS), pH 7.4 were of analytical grade.

General Measurements

FTIR spectra were registered on a VERTEX 70 BRUCKER FTIR spectrometer equipped with an ATR accessory. All FTIR measurements were performed in the ATR-FTIR cell on Ge crystal, at room temperature. The FTIR spectra were recorded using 32 scans in 600–4000 cm^{-1} wavenumber region. X-ray diffraction (XRD) patterns were recorded on a Panalytical X'PERT PRO MPD X-ray diffractometer with Cu Kα radiation. The scanning speed was 0.6/min, and the measurement range was $2\theta = 5$–$50°$. XRD analysis was conducted to study changes in the crystallinity of the scaffolds. UV-VIS spectroscopy was performed on a CINTRA 101 (GBC Scientific Equipment Pty.) double-beam spectrometer, using the wavelength scan method. TGA results were achieved on a Q500 TA instrument. A typical sample was heated from 20 to 700°C at a heating rate of 10°C/min under a constant nitrogen flow rate (balance flow 10 mL/min, oven flow 90 mL/min). DSC curves were registered on a Netzsch DSC 204 F1 Phoenix equipment, using a heating rate of 10°C/min. The sample was heated from 20 to 300°C under a constant nitrogen flow rate (20 mL/min). SEM was performed with a QUANTA INSPECT F SEM device equipped with a field emission gun with a resolution of 1.2 nm; gold coating was performed for enhanced surface conductivity. A Universal Testing Machine, Instron 3382 instrument, equipped with a 2 kN load cell at ambient temperature was used to estimate the mechanical properties of the samples. Cylindrical scaffolds measuring 12 mm in diameter and 4 mm in thickness were used for the tests. The samples were presoaked in PBS for 2 h and then they were examined at a cross-head speed of 1 mm/min. All the measurements were performed in triplicates the average value was calculated and reported. Next, the compressive stress (kPa) corresponding to each strain (%) was plotted.

Methods

Synthesis of Collagen-Sericin Scaffolds. To determine the molecular weight of SS powder sodiumdodecylsulfate-polyacrylamide gel electrophoresis (SDS-PAGE) was performed. The results indicate that SS contains peptides with molecular weights ranging from 30 to 40 kDa. Different values of the molecular weight of SS are reported in literature due to various extraction methods.[10,13]

Collagen-sericin scaffolds (Coll-SS) with variable concentration of SS and constant Coll content (see Table I for details) were prepared as follows. Briefly, the appropriate amount of SS was dissolved in 1 mL distilled water and further added to 8 mL Coll gel. 1 mL GA solution (0.5% reported to the weight of dry collagen) was added for *in situ* crosslinking. The resulting gels were then cast in polystyrene dishes and kept at 4°C for 24 h. They were washed with distilled water and freeze-dried for 48 h

Table I. The Scaffolds Compositions

No.	Samples	Coll : SS (wt/wt)	T%[a] (wt/v)
1	Coll	5 : 0	1.2
2	Coll-SS1	5 : 1	1.44
3	Coll-SS2	5 : 2	1.68
4	Coll-SS3	5 : 3	1.92
5	Coll-SS4	5 : 4	2.16
6	Coll-SS5	5 : 5	2.4

[a]T = total solid content expressed as total weight per volume of solution.

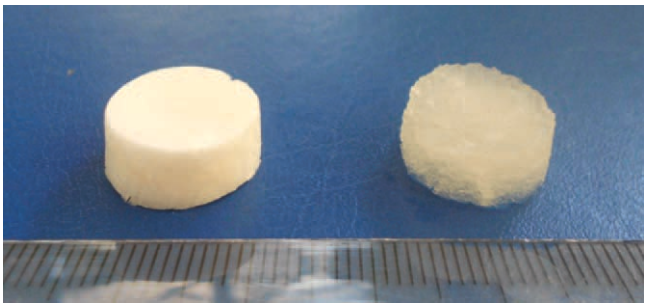

Figure 1. Typical appearance of porous Coll-SS4 scaffold in both dry and hydrated state. [Color figure can be viewed in the online issue, which is available at wileyonlinelibrary.com.]

to obtain porous scaffolds as follows: cooling to −40°C (4 h), keeping at this temperature for 5 h, then freeze-dried at −40°C and 0.12 mbar for 10 h. Then they were heated to +20°C at a rate of 3°C/h (20 h) at 0.12 mbar followed by heating (6 h) to 30°C at a rate of 2°C/h and finally freeze-dried at same temperature at 0.01 mbar for 3 h, using the Christ Model Delta 2–24 LSC freeze-dryer (Germany). 3D porous Coll-SS scaffolds were thus obtained as it can be seen from Figure 1.

Characterization of the Scaffolds. ATR-FTIR spectra were recorded for Coll-SS scaffolds, pure Coll scaffold and neat SS. XRD was performed to reveal the crystallinity of such scaffolds. To further investigate the effect of SS on the Coll-SS structures, the thermal behavior was revealed by TGA and DSC tests. SEM was used to investigate the morphological structure of the scaffolds.

A conventional gravimetric procedure was used to determine the SR of the investigated scaffolds.[32] The swelling behavior was determined by immersing samples in double-distilled water at 37°C. At scheduled time intervals, the samples were withdrawn, wiped (to remove the surface water) and weighed in the swollen state. The experiments were repeated four times under the same conditions and the average values were reported. SR was calculated using the following equation:

$$\%SR = \frac{Wt - Wi}{Wi} \times 100 \quad (1)$$

where, W_t denotes the weight of the swollen samples at immersion time t, and W_i denotes the weight of the dry samples. To further assess the effect of pH and ionic strength of external solvent on the swelling properties of the scaffolds, the maximum swelling ratio (MSR) was determined in PBS of pH 3, 7.4, and 11, as the equilibrium value established after 24 h.

The mechanical properties of the obtained superporous hydrogels were further estimated through compression tests. All the scaffolds were totally hydrated in distilled water prior testing. Furthermore, the integral stabilities of the obtained scaffolds were investigated by studying the *in vitro* release of the SS according to Aramwit et al.[19] The samples (Ø 1cm) were immersed into 10 mL distilled water at room temperature. Sample aliquots were extracted at different times 1 h, 4 h, 6 h, 24 h, 72 h, 120 h, 168 h, 336 h, 504 h, and 672 h and the absorbance was measured at 562 nm. The amount of protein released was compared with a BSA standard curve. All experiments were performed in triplicate. Enzymatic degradation of collagen scaffolds was also investigated by monitoring the mass loss of scaffolds as function of exposure time to a collagenase solution according to a procedure described in the literature.[33,34] Pieces of collagen scaffolds (1 cm in diameter) were accurately weighed (wet weight without excess of water), placed in a solution of PBS and collagenase (1 μg/mL) at pH 7.4, and incubated at 37°C. At regular intervals, the swollen scaffolds were removed from the collagenase solution, wiped and weight. The percent of degradation of matrices was determined using Equation (2):

$$\%\ \text{weight loss} = Wt - Wi/Wi \times 100, \quad (2)$$

where, W_i is the initial weight and W_t is the weight after time t. Each biodegradation experiment was repeated 5 times. The final percentage of biodegradation was calculated as the average values.

RESULTS AND DISCUSSION

Spectral Characterization

ATR-FTIR spectra successfully confirmed the composition of the scaffolds. Figure 2 shows the ATR-FTIR spectra of the Coll-SS scaffolds and of the raw materials.

Neat SS exhibits the characteristic absorption bands at 3299 cm^{-1} (O—H and amide N—H stretching vibration), 1646 cm^{-1} (amide I), 1531 cm^{-1} (amide II) and 1242 cm^{-1} (amide III). These bands are very useful for estimating protein secondary structure and are typically assigned to a disordered structure because SS exhibits a random coil conformation.[22,35]

Instead Coll shows its characteristic vibrations at 3323 cm^{-1} (stretching vibrations of O—H and N—H bonds from both amides and primary amines), 1650 cm^{-1} (amide I), 1554 cm^{-1} (amide II), and 1240 cm^{-1} (amide III). Typical for Coll a band is observed at 1451 cm^{-1} due to the pyrrolidine ring of hydroxyproline residues. This vibration is not significant in SS due to the low concentration of this amino acid in the peptide chain. The recorded bands for Coll perfectly matched with data reported in the literature.[36–40]

On the other hand, an essential parameter for the presence of triple helix structure is A_{III}/A_{1451} defined as the ratio between the areas of amide III and 1451 cm^{-1} bands. Andrews et al.[41] showed that if the value of $A_{III}/A_{1451} \geq 1$ then the triple helix is confirmed. Considering this, the calculated value for the Coll used in this work was 1.01 this proving the existence of a triple helix configuration. The ratios A_{III}/A_{1451} for the Coll-SS scaffolds are not relevant any more for the nature of Coll as in these materials the signal for amide III has a double origin: Coll and SS.

Further on, the spectra of the mixed Coll-SS scaffolds indicate a right-shifting of two of the main peaks when compared with the raw materials (Figure 2). Thus, the broad vibration at 3323 cm^{-1} in Coll is shifted to 3315 cm^{-1} in sample Coll-SS1 and to 3302 cm^{-1} in sample Coll-SS5. Nevertheless, the shape of this signal directly depends on the composition of each scaffold as it is the result of overlapping vibrations of O—H and N—H bonds. In the same time, the maximum for amide II shifts from

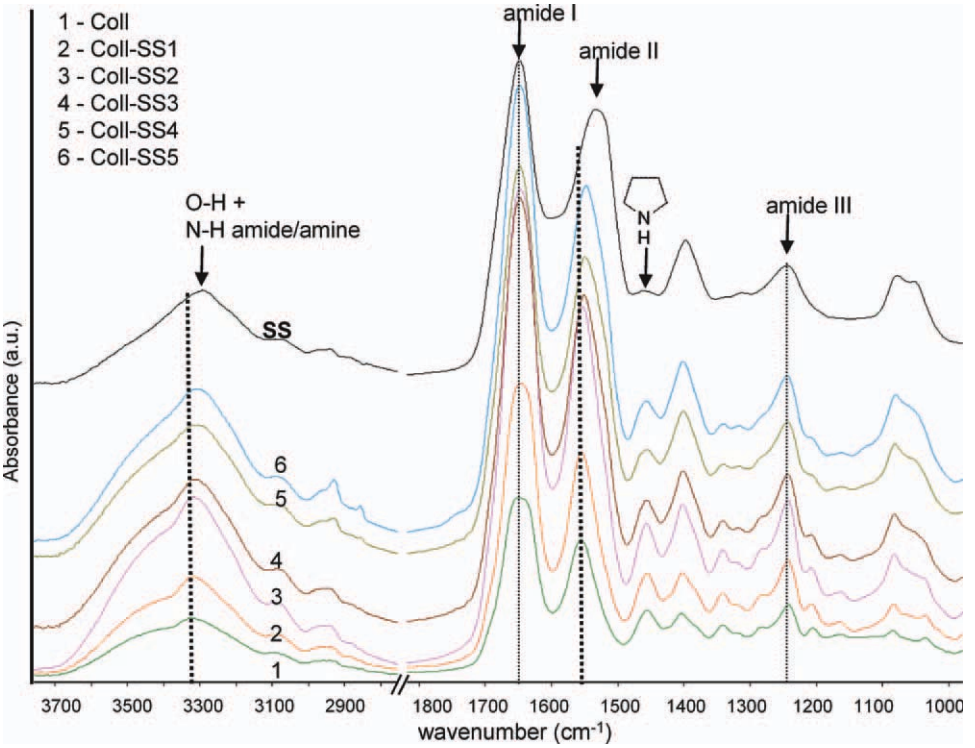

Figure 2. ATR-FTIR spectra of SS and Coll-SS scaffolds. The specific vibrations of Coll are indicated with dash lines to better visualize the shifting with increasing SS loading. [Color figure can be viewed in the online issue, which is available at wileyonlinelibrary.com.]

1554 cm^{-1} in Coll to lower wavenumbers like 1551 cm^{-1} in sample Coll-SS2 and to 1545 cm^{-1} in sample Coll-SS5. The shifting of bands at 3323 cm^{-1} and 1554 cm^{-1} in Coll confirms the increased SS content within the scaffolds but also possible interactions between Coll and SS through hydrogen bonds.

Figure 3 presents the results of crystallographic analysis (XRD) for all the porous scaffolds that were prepared using the same Coll concentration and various SS contents. The obtained diffractograms were compared with the XRD patterns of pure Coll scaffold and neat SS.

The XRD profiles showed that the obtained materials exhibit typical patterns of amorphous phase with the absence of crystallinity peaks. For the pure Coll scaffold some crystalline halos at $2\theta = 8.3°$ and 18° could be observed indicating a tendency to structural organization. SS showed a weak and wide pattern with a maximum 2θ around 20.9° with a spacing of 4.8 Å due to noncrystalline form as the typical characteristic diffraction pattern of amorphous SS. To date, most experimental evidences indicate that the secondary structure of SS is mainly amorphous (random coil) and contains few β-sheets, but lacks α-helix, so

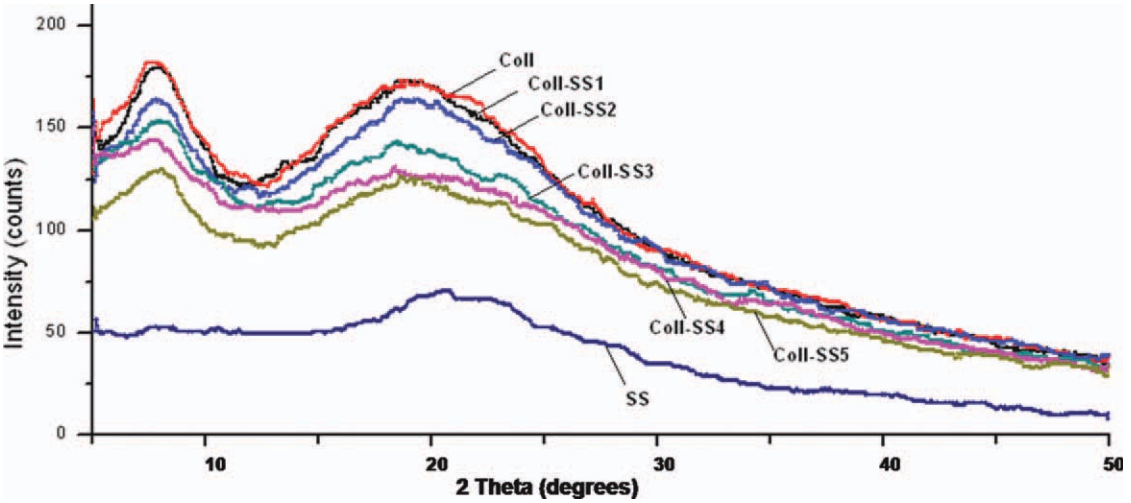

Figure 3. XRD diffractograms of Coll-SS scaffolds. [Color figure can be viewed in the online issue, which is available at wileyonlinelibrary.com.]

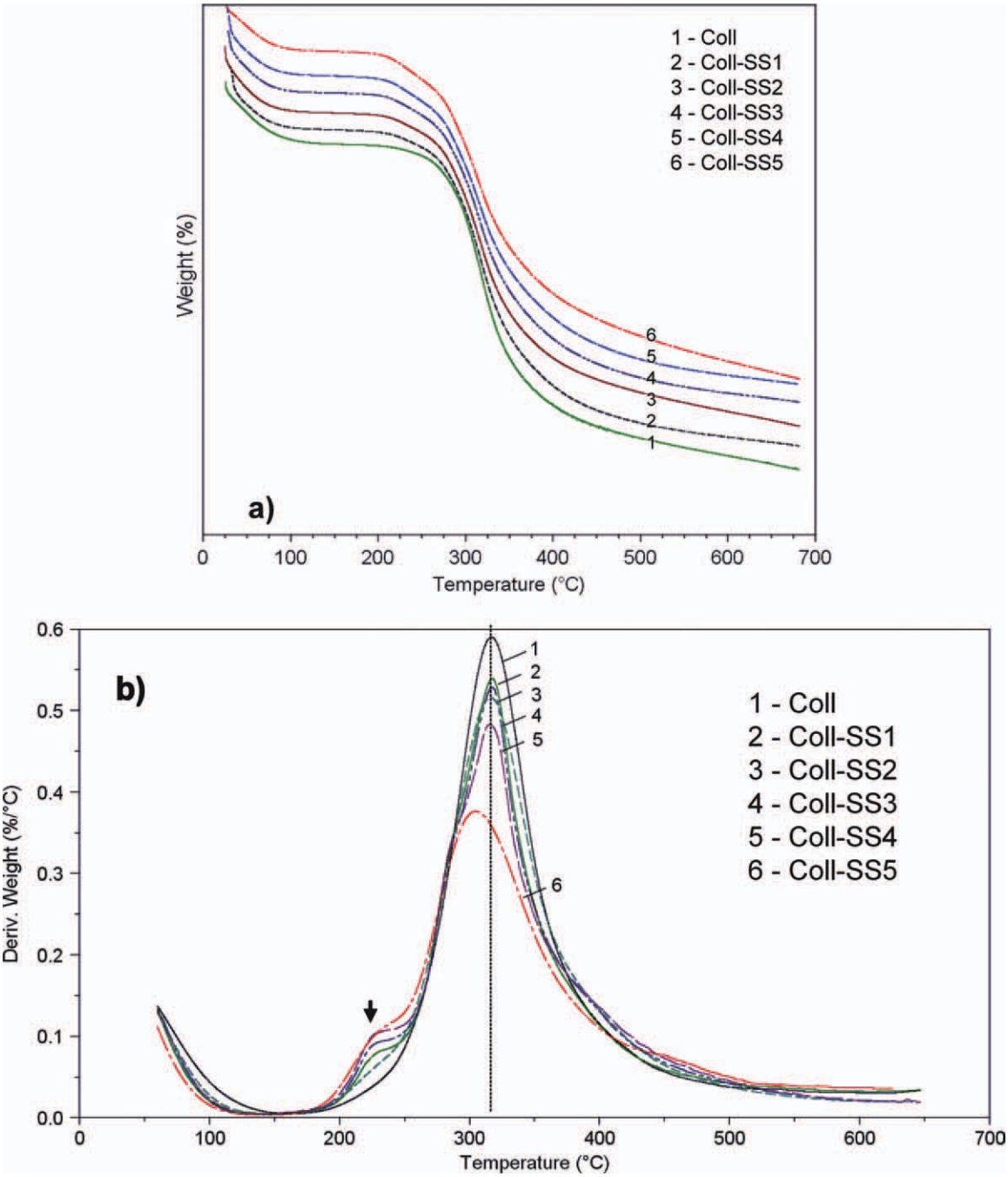

Figure 4. TGA (a) and DTG (b) curves of Coll-SS scaffolds. [Color figure can be viewed in the online issue, which is available at wileyonlinelibrary.com.]

X-ray analysis is not very efficient for SS because of its low crystallinity. The XRD patterns of prepared porous SS materials reveal a major peak around 19.5° and a minor peak around 8.4°. The intensity of these halos decreases with SS loading due to the fact that SS alters the diffraction signature from the Coll helix.

Figure 4 shows TGA (a) and DTG (b) curves of Coll-SS scaffolds with an increased amount of SS.

The thermograms of all samples showed similar profiles. The initial weight loss of samples observed around 100°C is due to loss of moisture while the second weight loss, in a temperature range of 200–400°C, is associated with the breakdown of side chain groups of amino acid residues, as well as the cleavage of peptide bonds from the proteins[27] [Figure 4(a)]. It should be also noted that the residual mass at 700°C gradually increases at higher levels of SS because of the neat SS which exhibits a lower weight loss (65%) (data not shown) than simple Coll (73% weight loss).

DTG curves clearly show one main decomposition peak (around 310°C) assigned to the thermal degradation of crystalline regions from both Coll and SS proteins [Figure 3(b)]. As

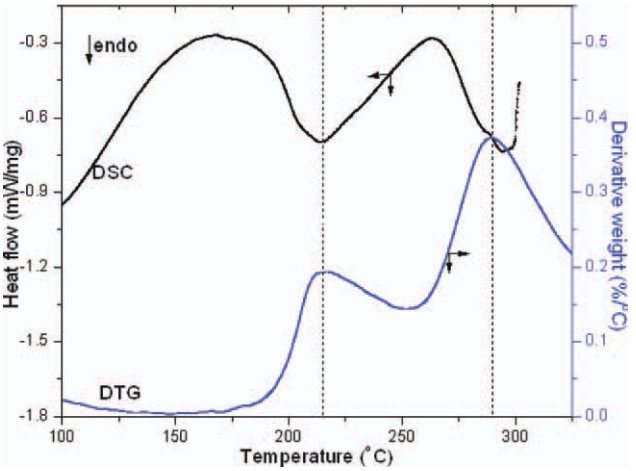

Figure 5. Overlay plot of DSC and DTG curves for neat sericin. [Color figure can be viewed in the online issue, which is available at wileyonlinelibrary.com.]

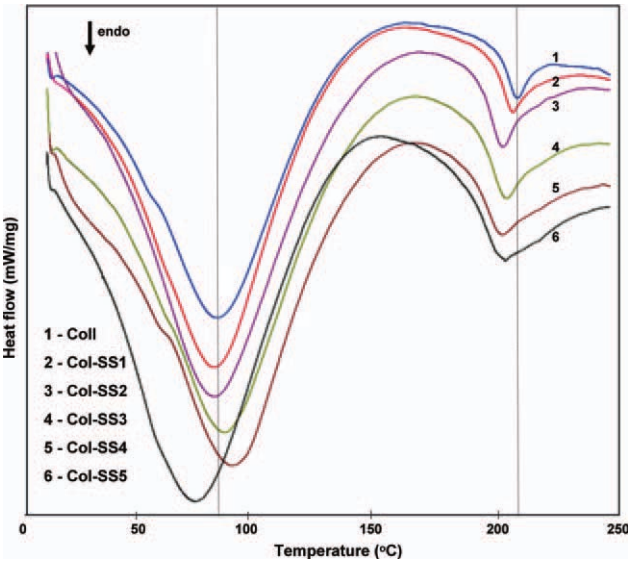

Figure 6. DSC curves for Coll-SS scaffolds. [Color figure can be viewed in the online issue, which is available at wileyonlinelibrary.com.]

the SS amount increases this peak is slightly shifted toward lower temperatures (318°C for Coll-SS1 to 305°C for Coll-SS5).

Moreover, as the SS amount increases a second peak appears (around 215°C) characteristic to SS as it will be further observed from Figure 5. DTG curve exhibits two maximum degradation events at 215 and 290°C which correspond to the thermal degradation of the amorphous and crystalline domains, respectively. This fact also demonstrates the downward shifting of the peak assigned to the thermal degradation of the crystalline regions from both Coll and SS from Coll-SS scaffolds as it was previously mentioned. The thermal behavior of neat SS was additionally proved using DSC analyses. For a better visualization DSC plot was presented in overlay with the DTG thermogram (Figure 5). The two peaks observed in DTG curve fully overlap the endothermic peaks displayed in DSC thermogram.

More details about the thermal behavior of Coll-SS scaffolds can be revealed from the DSC curves (Figure 6).

On the DSC thermograms two distinct endothermic peaks were identified. All analyzed samples exhibit similar behavior suggesting the good miscibility between Coll gel and SS solution in the resulting freeze-dried scaffold.

Under the influence of heating all studied scaffolds exhibit a broad endothermic peak around 90°C due to an advanced dehydration. The obtained results are in good agreement with those reported for Coll and SS separately investigated.[42–45] According to our data, as the SS content increases, this peak is shifted to higher temperatures compared with Coll (from 92°C up to 100°C) probably due to an increased number of hydrogen bonds, established between the Coll and SS molecules, which partially hinders the dehydration of Coll. However at a high quantity of SS (in Coll-SS5 scaffold) the hydrogen bonds are more likely to be formed between the SS molecules rather than between SS and Coll. Thus the dehydration of Coll is more facilitated so that the peak shifted to lower values (88°C). Therefore, the competition of hydrogen bonds formation between SS and Coll and SS itself is a key factor which influences the thermal transitions (Figure 7).

Increasing the temperature, DSC curves exhibit a supplementary endothermic peak around 220°C, which is assigned to the melting temperature (T_m) of the amorphous domains from both proteins Coll and SS.[27,46,47] This melting/decomposition temperature decreases gradually as the SS content increases due to a lower thermal resistance of SS (215°C) with respect to native Coll scaffold (221°C). As SS is loaded the amorphous phase consecutively increases leading to a less ordered structure of the scaffolds and thus the thermal degradation starts earlier (from

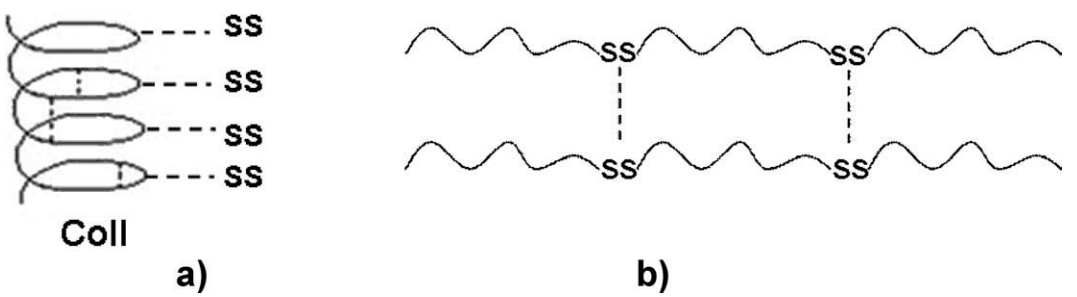

Figure 7. Hydrogen bonds between Coll and SS (a) and between SS molecules (b).

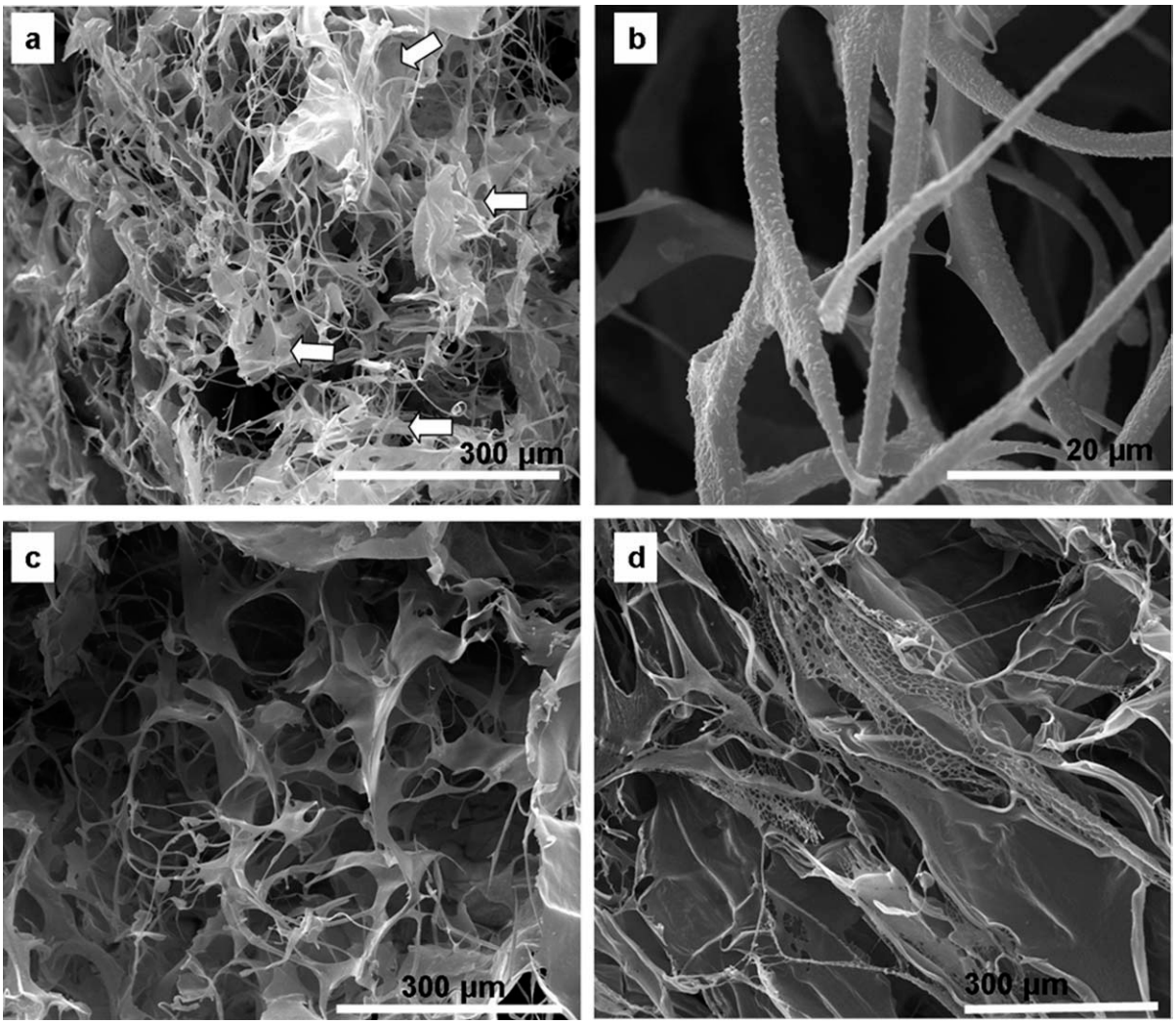

Figure 8. SEM images of Coll scaffold: (a) general view; (b) detail of entangled fibrils (approximately 1 μm diameter); white arrows indicate ribbon-like structures. SEM images of Coll-SS1: (c) entangled fibrils forming round pores, and (d) ribbon-like structures.

219°C for Coll-SS1 to 217°C for Coll-SS3 and 215°C for Coll-SS5).

The morphology of the porous scaffold is very important because it affects a series of characteristics like the water uptake capacity and the mechanical properties. Nevertheless, the chemical degradation of the porous materials depends directly on the porosity.

In this context, the morphology was evaluated using SEM images. In Figure 8(a,b) it can be observed that Coll used as reference material in this study appears as a highly porous network with pores formed through the entanglement of fibrils. Ribbon-like structures are occasionally observed. Introducing SS in the scaffold modifies the porosity of the materials as further shown [Figure 8(c,d)]. The matrix with the lowest SS content exhibits two types of internal architectures. Fibrillar structures are still present [Figure 8(c)] similar to those characteristics to Coll. Through the interconnections of these fibrils an external shell of the material is formed, with ring-like pores ranging from 60 to 130 μm. The core consists in multilayered ribbons and denser meshes as shown in Figure 8(d).

Further increasing SS concentration generates more homogenous porous scaffolds. It should be also remembered that increasing SS amount corresponds to augmenting of the total solid content as shown in Table I. This is very important as all the morphological changes observed represent the synergistic effect of the two above mentioned compositional factors. Thus, each Coll: SS ratio leads to a different porosity, but keeping the same tendency to generate a sponge-like network with increasing homogeneity.

Thus, Coll-SS2 scaffold [Figure 9(a)] appears as spongeous structure with round cavities of different diameters, from 50 to 90 μm. Separation walls with multiple holes start to be distinguished as very thin structures. The morphology of Coll-SS3 [Figure 9(b)] is very similar to that of Coll-SS2, but the material is denser, the separation walls become thicker and the pores decrease in diameter to approximately 35–80 μm.

Applied Polymer SCIENCE

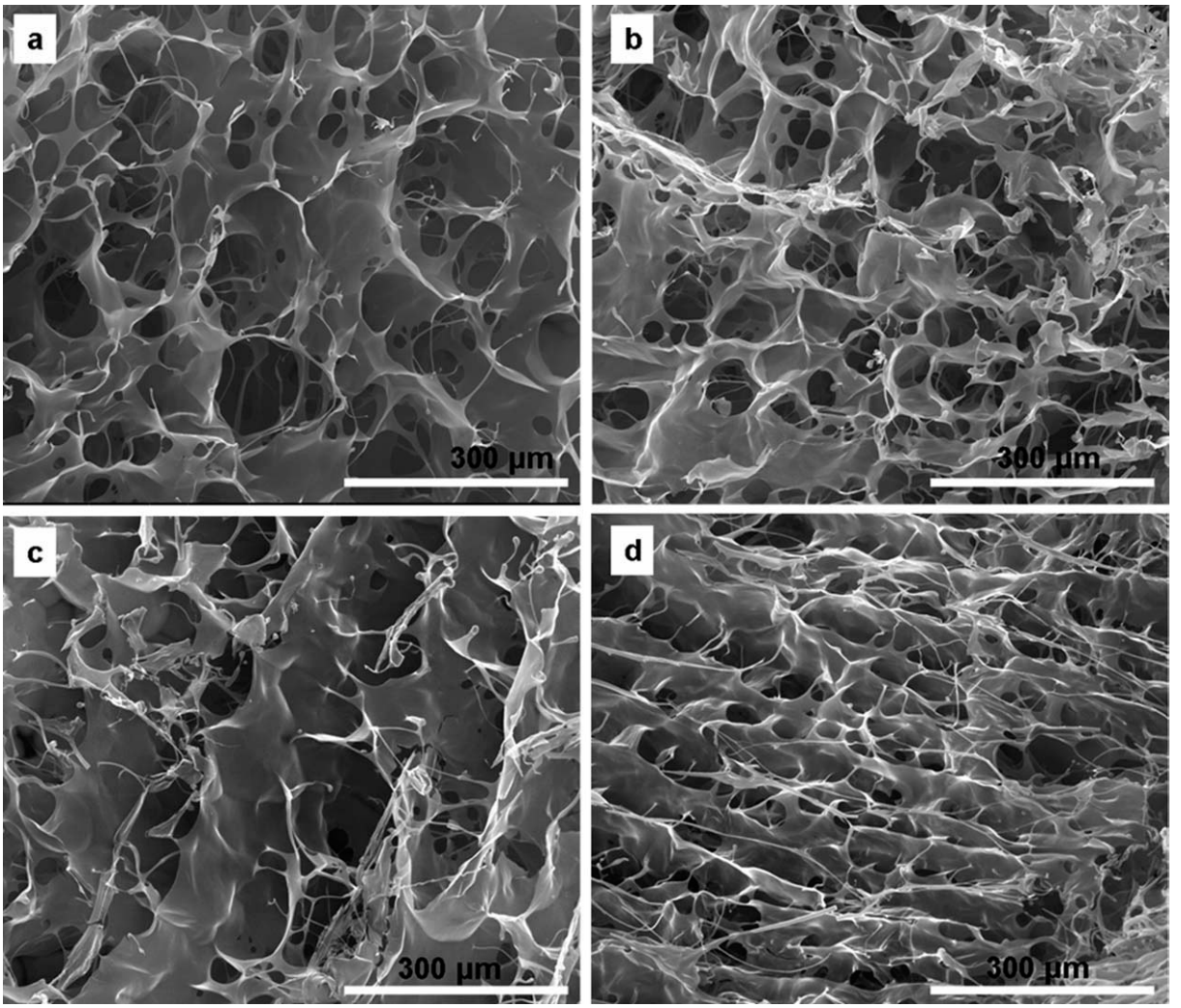

Figure 9. General morphology of Coll-SS2 (a), Coll-SS3 (b), Coll-SS4 (c), and Coll-SS5 (d) as obtained by SEM.

If Coll: SS ratio $\leq$ 1 and the total solid content is above 2%, the morphology changes again, remaining homogenous as general appearance but presenting multilayered structures connected by fibrillar pillars [Figure 9(c,d)]. These layers become more tightly packed in Coll-SS5 when compared to Coll-SS4. Nevertheless, these materials exhibit a different porosity, consisting in the free volume between the pillars and the continuous layers. The sizes range from 25–70 μm in Coll-SS4 to 2–35 μm in Coll-SS5. These architectural features strongly depend on the composition of the scaffolds and will further influence the wettability, swelling, and degradation of the materials.

The swelling properties of biomaterials are very important when aiming biomedical applications. The water uptake is a key factor for the surface and mechanical properties of hydrogels. In the same time, it influences the eventual loading/release of bioactive species in/from these materials as well as the degradative processes.

The water uptake was monitored for an extended period of time till equilibrium was achieved and it was found to be affected by both morphological and compositional factors (Figure 10).

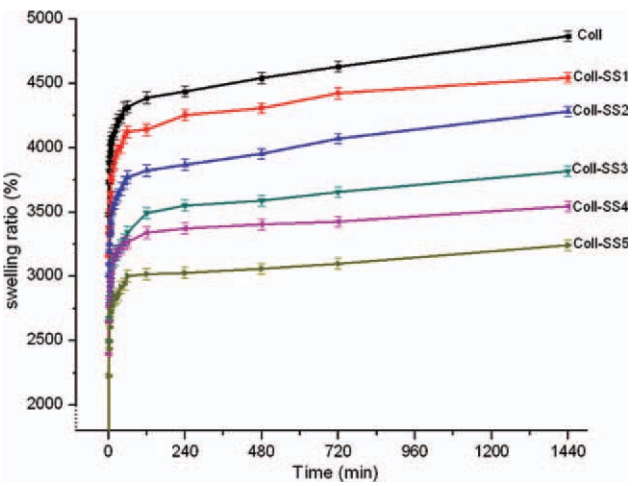

Figure 10. SW in water versus time for Coll-SS scaffolds and Coll control. [Color figure can be viewed in the online issue, which is available at wileyonlinelibrary.com.]

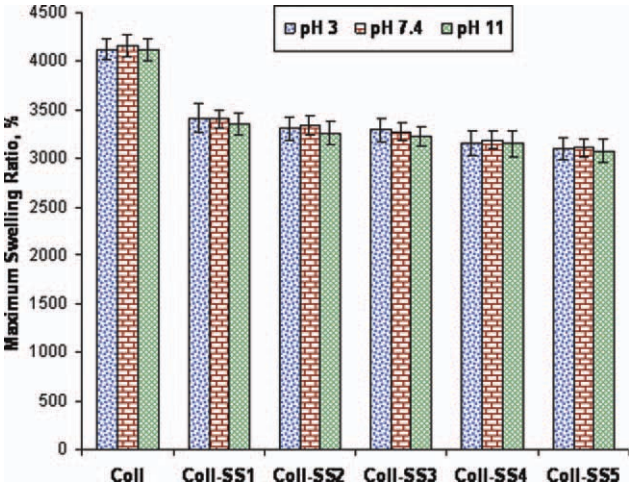

Figure 11. MSR of Coll-SS scaffolds after 24 hours at pH 3, 7.4, and 11. [Color figure can be viewed in the online issue, which is available at wileyonlinelibrary.com.]

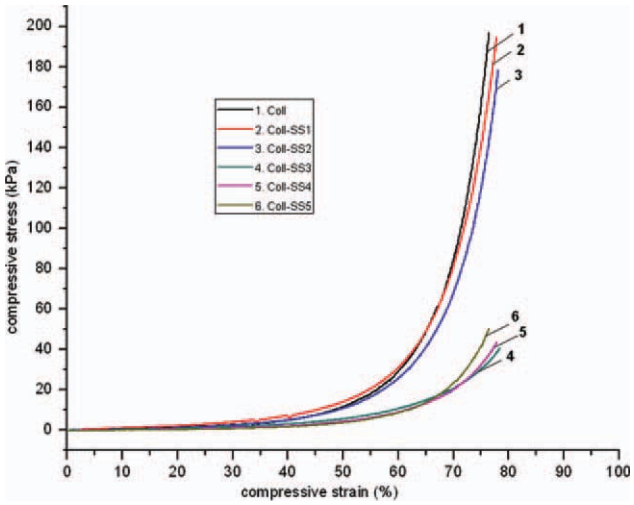

Figure 12. Effects of different SS content on mechanical properties of Coll:SS gels. [Color figure can be viewed in the online issue, which is available at wileyonlinelibrary.com.]

The presence of SS in the materials decreases the swelling tendency when compared with the control Coll scaffold. It is obvious that interconnected pores forming a foam-like structure enhance water uptake and thus facilitate swelling occurrence, while denser materials reduce water uptake capacity. Thus, in a first view, it was observed that all the materials reach MSR (expressed as the maximum value of the SW) very fast (approximately 90% in the first hour). This behavior is mainly due to the 3D porous structure of the matrices facilitating the penetration of water into the scaffold. The hydrophilic nature of the two polymer components and the ratio between them also contributed.

On the other hand, when comparing the values of the MSR (Figure 10), it can be noticed that increasing SS content leads to lower values. The decrease is significant when compared with Coll scaffold. Increasing SS when the ratio Coll: SS >1 is associated to moderate decrease of MSR values (4500 $\pm$ 125% for Coll-SS1, 4200 $\pm$ 100% for Coll-SS2, and 3800 $\pm$ 140% for Coll-SS3). This is also in agreement with the morphological features previously described. Further increase of SS content when Coll: SS ≤ 1 simultaneously with the total solid content (T $>$ 2%) leads to even lower MSR (3500 $\pm$ 210% for Coll-SS4 and 3200 $\pm$ 180% for Coll-SS5). This is normal as these compositions are associated with denser materials, more tightly packed and with smaller pores. Moreover, the results of the swelling tests in correlation with the porosity assessed by SEM confirm the superporous nature of the Coll-SS scaffolds.

With respect to the potential biomedical applications of these scaffolds, the swelling equilibrium values at the end of 24 h (MSR % in Figure 11) are presented for different pH values. It was noticed that the equilibrium values are not influenced by the solvent pH and ionic strength. Furthermore, a lower swelling response with increasing SS content was identified to be similar with the swelling tendency in double-distilled water.

The next objective was to determine the mechanical properties of the investigated superporous hydrogels. First, all the scaffolds were totally hydrated in distilled water prior testing. It is known that in the swollen state physical entanglements are nearly nonexistent and consecutively the strength of the material depends almost entirely of the crosslinking density. Figure 12 depicts the compressive stress versus strain curves of the Coll-SS scaffolds in the swollen state.

From the curves, it can be easily observed the effect of different SS content on the mechanical properties of hydrogels. As shown in Figure 12, the stress and strain of Coll-SS1 and Coll-SS2 are very close to that of Coll. This result indicates that small amounts of SS do not affect the mechanical properties of Coll hydrogels. The compressive stress significantly decreases with increasing SS content from 180 kPa for Coll-SS3 to about 40 kPa for Coll-SS4, Coll-SS5, and Coll-SS6. This fact could be assigned to the amorphous nature of SS, a higher content of this protein in matrices reduces the mechanical strength of the

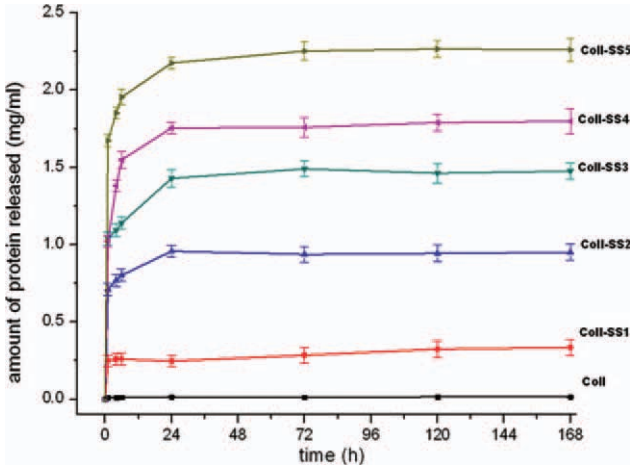

Figure 13. The amount of protein released from the synthesized scaffolds. [Color figure can be viewed in the online issue, which is available at wileyonlinelibrary.com.]

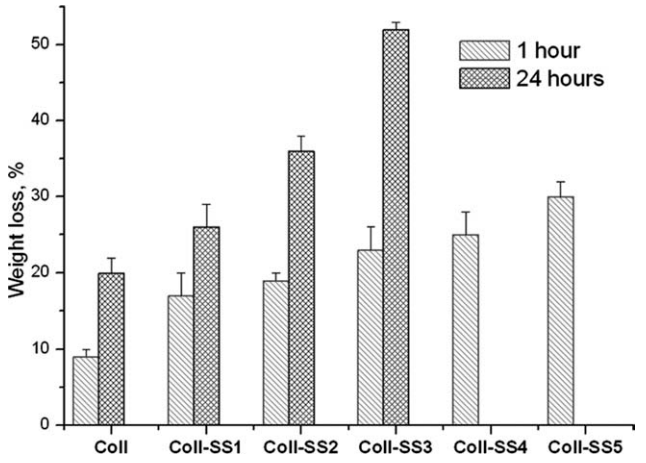

Figure 14. *In vitro* degradation behavior shown after collagenase treatment for 24 h.

Coll: SS scaffolds. This outcome is absolutely consistent with the conclusions mentioned above in XRD or thermal analysis sections.

The stability of the scaffolds was assessed both in distilled water and through enzymatic attack as further presented. In a first step, it was noticed that the amount of protein released in water increases in time, reaching stability in approximately 24 h (Figure 13). Very important, Coll proved to be stable in water for 7 days, while a strong positive influence of SS content on the protein release was observed. Therefore, it seems that SS is the main released component. Accordingly, Coll-SS5 releases approximately seven times more protein when compared with the sample with the lowest SS content (Coll-SS1). These results indicate a strong composition-stability/degradability dependency. Furthermore, releasing SS could have beneficial effects on collagen production in wounds as previously suggested by Aramwit et al.[19]

Then, the analysis of the structure/properties relationship was continued by *in vitro* degradation of the materials using collagenase. The control of degradation rate of the scaffolds is an important feature, as the *in vivo* resorption influences tissue regeneration ability. Collagen can be fully digested only by collagenases that are distinctive enzymes as they are able to cleave collagen triple helical region under physiological conditions of pH and temperature. The results of *in vitro* degradation performed with collagenase in PBS, 7.4 pH at 37°C are presented in Figure 14. The degradative process starts with the penetration of the enzyme inside the polymer matrices. The network of interconnected pores as well as the fast swelling (MSR was reached in only 1 hour) facilitates the fast attack of the enzyme. Thus, Coll presents a 10% weight loss after 1 h while Coll-SS materials lose between 18–30% of their mass in the same time interval. After 24 h, Coll lost ~ 20% of its mass while SS-containing materials present more important weight losses, ranging from 25% in Coll-SS1 to total collagen digestion in Coll-SS4 and Coll-SS5.

This behavior could be attributed to the SS component acting as a diluent of the Coll network. Increasing SS corresponds to decreasing Coll density in the network and enhances the degradation process in terms of degradation rate.

Therefore, SS exhibits a strong influence on the stability of the Coll-SS scaffolds leading to superporous materials which degrade faster. This behavior can be further considered an advantage or disadvantage depending on the targeted application.

CONCLUSIONS

Novel superporous scaffolds based on two proteins, collagen, and sericin were synthesized using various ratios between the two components. SS content strongly influences the structure-properties relationship. All the morphological changes observed using SEM represent the synergistic effect of the SS loading and of the augmenting of the total solid content. The architectural features in correlation with the results of the swelling tests confirm the superporous nature of the Coll-SS scaffolds and strongly influence the *in vitro* degradation of the materials. Furthermore, the mechanical properties can be easily tuned by increasing the crosslinking density to make the material suitable for different biomedical applications.

ACKNOWLEDGMENTS

This work was supported by CNCSIS–UEFISCSU, project number PNII–IDEI code 248/2010.

REFERENCES

1. Malafaya, P. B.; Silva, G. A.; Reis, R. L. *Adv. Drug. Deliv. Rev.* **2007,** *59*, 207.
2. Berisio, R.; Vitagliano, L.; Mazzarella, L.; Zagari, A. *Protein Pept. Lett.* **2002,** *9*, 107.
3. Brodsky, B.; Ramshaw, J. A. *Matrix. Biol.* **1997,** *15*, 545.
4. Trandafir, V.; Popescu, G.; Albu, M. G.; Iovu, H.; Georgescu, M. Collagen Based Bioproducts; Ars Docendi Press: Bucharest, **2007;** Chapter 2, pp 80–85.
5. Albu, M. G. Collagen Gels and Matrices for Biomedical Applications; Lap Lambert Academic Publishing GmbH & Co. KG: Saarbrücken, **2011;** Chapter 2, pp 6–12.
6. Lungu, A.; Albu, M.; Trandafir, V. *Mat. Plast.* **2007,** *44*, 273.
7. Titorencu, I.; Jinga, V.; Lungu, A.; Trandafir, V.; Albu, M. G.; Rau, I.; Iovu, H. *Mol. Cryst. Liq. Cryst.* **2008,** *486*, 1189.
8. Flocea, P.; Verestiuc, L.; Popa, M.; Sunel, V.; Lungu, A. *J. Macromol. Sci. Part. A Pure Appl. Chem.* **2010,** *47*, 616.
9. Zhang, Y. Q.; Tao, M. L.; Shen, W. D.; Mao, J. P.; Chen, Y. *J. Chem. Technol. Biotechnol.* **2006,** *81*, 136.
10. Zhang, Y. Q. *Biotechnol. Adv.* **2002,** *20*, 91.
11. Padamwar, M. N.; Pawar, A. P. *J. Sci. Ind. Res.* **2004,** *63*, 323.
12. Aramwit, P.; Kanokpanont, S.; De-Eknamkul, W.; Kamei, K.; Srichana, T. *J. Biomater. Sci. Polym. Ed.* **2009,** *20*, 1295.
13. Aramwit, P.; Sangcakul, A. *Biosci. Biotechnol. Biochem.* **2007,** *71*, 2473.
14. Soong, H. K.; Kenyon, K. R. *Ophthalmology* **1984,** *91*, 479.

15. Panilaitis, B.; Altman, G. H.; Chen, J.; Jin, H. J.; Karageorgiou, V.; Kaplan, D. L. *Biomaterials* **2003,** *24*, 3079.
16. Aramwit, P.; Kanokpanont, S.; De-Eknamkul, W.; Srichana, T. *J. Biosc. Bioeng.* **2009,** *107*, 556.
17. Anghileri, A.; Lantto, R.; Kruus, K.; Arosio, C.; Freddi, G. *J. Biotechnol.* **2007,** *127*, 508.
18. Cho, K. Y., Moon, J. Y., Lee, Y. W., Lee, K. G., Yeo, J. H., Kweon, H. Y., Kim, K. H.; Cho, C. S. *Int. J. Biol. Macromol.* **2003,** *32*, 36.
19. Aramwit, P.; Siritientong, T.; Kanokpanont, S.; Srichana, T. *Int. J. Biol. Macromol.* **2010,** *47*, 668.
20. Yoshii, F.; Kume, N.; Makuuchi, K.; Sato, F. 06–017373A, Jpn. Pat. **2000.**
21. Kongdee, A.; Bechtold, T.; Teufel, L. *J. Appl. Polym. Sci.* **2005,** *96*, 1421.
22. Aramwit, P.; Damrongsakkul. S.; Kanokpanont, S.; Srichana, T. *Biotechnol. Appl. Biochem.* **2010,** *55*, 91.
23. Tsukada, M.; Arai, T.; Colonna, G. M.; Boschi, A.; Freddi, G. *J. Appl. Polym. Sci.* **2003,** *89*, 638.
24. Ki, C. S.; Kim, J. W.; Oh, H. J.; Lee, K. H.; Park, Y. H. *Int. J. Biol. Macromol.* **2007,** *41*, 346.
25. Nomura, M.; Iwasa, Y.; Araya, H. 07–292240A, Jpn. Pat. **1995.**
26. Kearns, V.; MacIntosh, A. C.; Crawford, A.; Hatton, P. V. In Topics in Tissue Engineering; Ashammakhi, N.; Reis, R.; Chiellini, F., Eds.; **2008,** Vol. *4*, Chapter 1, pp 1–19.
27. Zhang, H.; Deng, L.; Yang, M.; Min, S.; Yang, L.; Zhu, L. *Int. J. Mol. Sci.* **2011,** *12*, 3170.
28. Minoura, N.; Aiba, S. I.; Gotoh, Y.; Tsukada, M.; Imai, Y. *J. Biomed. Mater. Res.* **1995,** *29*, 1215.
29. Tsubouchi, K.; Igarashi, Y.; Takasu, Y.; Yamada, H. *Biosci. Biotechnol. Biochem.* **2005,** *69*, 403.
30. Mandal, B. B.; Priya, A. S.; Kundu, S. C. *Acta Biomater.* **2009,** *5*, 3007.
31. Akturk, O.; Tezcaner, A.; Bilgili, H.; Deveci, M. S.; Gecit, M. R.; Keskin, D. *J. Biosci. Bioeng.* **2011,** *112*, 279.
32. Mandal, B.B.; Kapoor, S.; Kundu, S.C. *Biomaterials,* **2009,** *30*, 2826.
33. Suri, S.; Schmidt, C. E. *Acta Biomater.* **2009,** *5*, 2385.
34. Song, E.; Kim, S. Y.; Chun, T.; Byun, H. J.; Lee, Y. M. *Biomaterials* **2006,** *27*, 2951.
35. Ogino, M.; Tanaka, R.; Hattori, M.; Yoshida, T.; Yokote, Y.; Takahashi, K. *Biosci. Biotechnol. Biochem.* **2006,** *70*, 66.
36. Figueiro, S. D.; Goes, J. C.; Moreira, R. A.; Sombra, A. S. B. *Carbohydr. Polym.* **2004,** *56*, 313.
37. Madhan, B.; Subramanian, V.; Rao, J. R.; Nair, B. U.; Ramasami, T. Int. *J. Biol. Macromol.* **2005,** *37*, 47.
38. Baia, L.; Baia, M.; Danciu, V.; Albu, M. G.; Cosoveanu, V.; Iordachescu, D.; Trandafir, V. *J. Optoelectron. Adv. Mater.* **2008,** *10*, 933.
39. He, L.; Mu, C.; Shi, J.; Zhang, Q.; Shi, B.; Lin, W. *Int. J. Biol. Macromol.* **2011,** *48*, 354.
40. Lin, S. Y.; Wei, Y. S.; Hsieh, T. F.; Li, M. J. *Biopolymers* **2004,** *75*, 393.
41. Andrews, M. E.; Murali, J.; Muralidharan, C.; Madhulata, W.; Jayakumar, R. *Colloid. Polym. Sci.* **2003,** *281*, 766.
42. Figueiro, S. D.; Mallmann, E. J. J.; Goes, J. C.; Ricardo, N. M. P. S.; Denardin, J. C.; Sombra, A. S. B.; Fechine, P. B. A. *Express. Polym. Lett.* **2010,** *4*, 790.
43. Davidenko, N.; Campbell, J. J.; Thian, E. S.; Watson, C. J.; Cameron, R. E. *Acta Biomater.* **2010,** *6*, 3957.
44. Pietrucha, K. *Int. J. Biol. Macromol.* **2005,** *36*, 299.
45. Tsereteli, G. I.; Belopolskaya, T. V.; Grunina, N. A. *J. Therm. Anal. Calorim.* **2008,** *92*, 711.
46. Lee, K. G.; Kweon, H. Y.; Yeo, J. H.; Woo, S. O.; Lee, Y. W.; Cho, C. S.; Kim, K. H.; Park, Y. H. *Int. J. Biol. Macromol.* **2003,** *33*, 75.
47. Budrugeac, P.; Badea, E.; Gatta, G. D.; Miu, L.; Comanescu, A. *Thermochim. Acta* **2010,** *500*, 51.